Chinese Chemical Letters 37 (2026) 110626

Contents lists available at ScienceDirect

Chinese Chemical Letters

journal homepage: www.elsevier.com/locate/cclet

In-situ construction and tuning of a poly(1,3-dioxolane) dual-interlayer electrolyte bolstering high performance of solid-state battery

Xiaojin Wang[a,1], Yi Chang[c,1], Yuanyuan Zhang[b,*], Zhuohua Li[a], Haiqi Huang[a], Yansha Huang[a], Jiawei Hu[a], Kai Zhang[d,*], Xuemei Gong[e], Ruirui Zhao[a,*]

[a] *School of Chemistry, National and Local Joint Engineering Research Center of MPTES in High Energy and Safety LIBs, Engineering Research Center of MTEES (Ministry of Education), and Key Lab. of ETESPG(GHEI), South China Normal University, Guangzhou 510006, China*
[b] *Analysis & Testing Center, Key Laboratory of Theoretical Chemistry of Environment Ministry of Education, South China Normal University, Guangzhou 510006, China*
[c] *GAC AION New Energy Automobile Co., Ltd., Guangzhou 511434, China*
[d] *Key Laboratory of Advanced Energy Materials Chemistry (Ministry of Education), Nankai University, Tianjin 300071, China*
[e] *Guangzhou TianTie Technology Research Co., Ltd., Guangzhou 510710, China*

ARTICLE INFO

Article history:
Received 26 September 2024
Revised 4 November 2024
Accepted 7 November 2024
Available online 8 November 2024

Keywords:
Solid-state battery
Interface modification strategy
In-situ polymerization
Garnet electrolyte
Poly(1,3-dioxolane)

ABSTRACT

Garnet-type ceramic $Li_7La_3Zr_2O_{12}$ (LLZO) stands out as a potential solid-state electrolyte, offering a promising alternative to conventional flammable liquid electrolytes. However, its large interfacial resistance with electrodes remains a significant challenge. In this research, we have successfully *in-situ* fabricated polymeric interface layers on both cathode and anode sides with LLZO. By tuning the gel-polymer interphase *via* fluoroethylene carbonate (FEC), known as FGPE, we have established a rapid Li^+ transport channel by enhancing the solid-solid interfacial contact. This FGPE layer exhibits exceptional ionic conductivity of 1.38 mS/cm and a high Li-ion transference number of 0.64. Furthermore, FGPE effectively mitigates concentration polarization under high currents, thereby enabling a higher capacity output. In comparison to gel-polymer interphases with dimethyl carbonate (DMC) as the solvent (referred to as GPE), the Li|FGPE|Li symmetrical cell has demonstrated superior stability in plating/strapping performance over 800 h at a current density of 0.1 mA/cm^2. Moreover, the Li|FGPE|LLZO|FGPE|$LiFePO_4$ cell has exhibited commendable rate capability and has maintained a high capacity retention of 98.94% at 0.5 C after 200 cycles. This study underscores an innovative approach in advancing in field of solid-state batteries, anticipated to be broadly applicable to other solid-state batteries by facilitating an abundance of robust solid-solid interfacial contacts.

© 2025 Published by Elsevier B.V. on behalf of Chinese Chemical Society and Institute of Materia Medica, Chinese Academy of Medical Sciences.

All-solid-state lithium metal batteries are poised to deliver high energy densities, presenting a compelling alternative to conventional liquid lithium-ion batteries. Solid-state electrolytes (SSEs) are recognized for their superior ionic conductivities and enhanced safety profiles, rivaling those of commercially available organic flammable liquid electrolytes [1–4]. Among these, the garnet-type $Li_7La_3Zr_2O_{12}$ (LLZO) is widely regarded as a particularly promising SSE [5]. However, the practical application of LLZO is impeded by its rigid surface, which leads to suboptimal electrode contact and elevated interfacial resistance.

Incorporating trace amounts of liquid electrolyte [6,7] or employing a polymer buffer layer [8,9] on the garnet ceramic electrolyte surface have been documented to ameliorate the interfacial connection. The conventional *ex-situ* casting technique, while effective in reducing interfacial resistance, presents new challenges such as increased solvent usage and heightened safety hazards [10]. Conversely, *in-situ* polymerization enables the transformation of liquid precursors into a gel state within the cell under ultraviolet or thermal conditions, thus creating a stable interface that promotes efficient Li^+ transport, prevents electrolyte leakage, and bolsters battery safety [11–13]. Given its exceptional flexibility, high ionic conductivity, and compatibility with lithium metal anodes [14–17]. Poly(1,3-dioxolane) (PDOL) is anticipated to serve as an effective intermediary between solid electrode and garnet LLZO electrolytes. However, the simultaneous resolution of anodic and cathodic interfacial issues in SSBs using PDOL is a relatively uncom-

* Corresponding authors.
E-mail addresses: yyzhang@m.scnu.edu.cn (Y. Zhang), zhangkai_nk@nankai.edu.cn (K. Zhang), zhaoruirui@m.scnu.edu.cn (R. Zhao).
[1] These authors contributed equally to this work.

https://doi.org/10.1016/j.cclet.2024.110626
1001-8417/© 2025 Published by Elsevier B.V. on behalf of Chinese Chemical Society and Institute of Materia Medica, Chinese Academy of Medical Sciences.

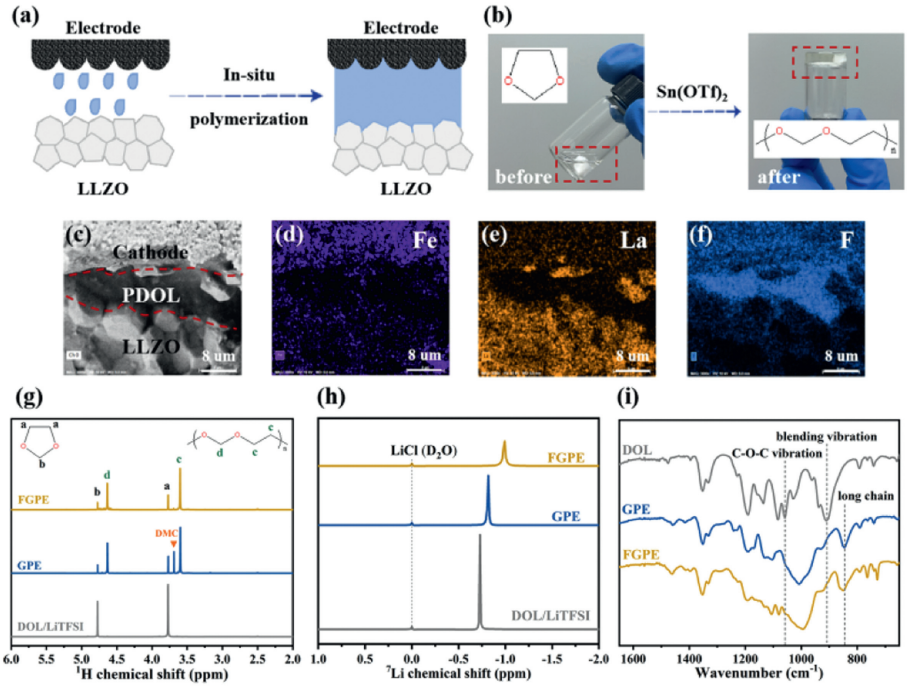


Fig. 1. A comprehensive analysis of the *in-situ* DOL polymerization process for electrode/LLZO interface modification. (a) Scheme of *in-situ* DOL polymerization for electrode/LLZO interface modification. (b) Optical images of DOL electrolyte solution prior to polymerization and the resultant gel-like PDOL with annotated chemical structures. (c) SEM cross-sectional diagrams of the cathode/LLZO interface in an assembled battery. (d-f) EDS mapping of Fe, La, and F elements at the interface. The characterization of DOL, GPE, and FGPE is further detailed through: (g) ^{1}H NMR spectra, (h) ^{7}Li NMR spectra, and (i) Fourier transform infrared spectra.

mon achievement, rendering the precise regulation of components both urgent and crucial to meet the high-performance demands of SSBs.

In this study, an *in-situ* polymerization method for 1,3-dioxolane (DOL) was proposed to tackle interfacial challenges. This method initiates the polymerization of DOL uniformly, leading to a substantial decrease in interfacial resistance. Furthermore, Floroethylene carbonate (FEC), serving as the solvent for polymerization initiator, was selected to replace DMC owing to its established role in optimizing the SEI film and enhancing flammability resistance in liquid-electrolyte batteries [18–21]. The findings reveal that the gel electrolyte incorporating FEC (FGPE) achieved an ionic conductivity of 1.38 mS/cm, surpassing the 0.68 mS/cm of the gel electrolyte incorporating DMC (GPE). The Li-ion transference number of FGPE, which is 0.64, indicates a substantial presence of free Li^{+} ions at the interface of LLZO and the electrodes, which is conducive to improved battery performance. The solid-state batteries fabricated with this approach maintained a capacity retention of 98.94% at 0.5 C after 200 cycles, underscoring the efficacy of the strategies proposed in achieving high-performance solid-state batteries.

As depicted in Fig. 1a, the DOL electrolyte is homogeneously dispersed at the electrode/LLZO interface prior to polymerization and is allowed to stand for 12 h at RT to ensure adequate contact between the electrode and LLZO. The DOL undergoes *in-situ* polymerization into PDOL, catalyzed by $Sn(OTf)_2$ through a ring-opening mechanism. The extent of polymerization is evidenced by the optical images before and after polymerization in the vitro experiments (Fig. 1b). Acting as a Lewis acid, the Sn^{2+} ion derived from $Sn(OTf)_2$ can accept the lone pair electrons from the oxygen atom in DOL, thereby facilitating ring-opening polymerization into a long-chain polymer [18]. This process effectively strengthens the cathode-electrolyte interface, forming a tight junction as observed in the cross-sectional SEM images of the assembled battery (Fig. 1c). Elemental mapping of Fe, La, and F elements (Figs. 1d-f) reveals a stratified interface, delineating the LFP cathode, PDOL, and LLZO layers, respectively. The *in-situ* formation of the gel-electrolyte not only diminishes impedance but also establishes a rapid Li^{+} transport pathway at the interface. The minimal fluidity of the gel-polymer electrolyte further prevents electrolyte leakage, enhancing the stability of the electrode/LLZO interface and overall battery safety.

The ring-opening polymerization of DOL is corroborated by NMR and FTIR analyses. The characteristic chemical shifts in the ^{1}H NMR spectrum (3.76 and 4.76 ppm) and ^{13}C NMR spectrum (94.3 and 64.1 ppm) correspond to the protons and carbons in the CH_2-CH_2-O and CH_2-O-CH_2 moities of the DOL cycloether monomer (Fig. 1g and Fig. S1 in Supporting information). Post-polymerization, the two ^{1}H peaks are upfield-shifted by 0.16 and 0.12 ppm, while ^{13}C peaks are downfield-shifted by 0.9 and 2.7 ppm, respectively [16,17,22]. The ratio of integrated PDOL to residual DOL peaks suggests a high degree of polymerization, resulting in a gel-like consistency. The presence of DMC and FEC is also detected and annotated in the figure. The FTIR spectrum in Fig. 1i further confirms the completion of DOL polymerization. The peaks at 914 and 1030 cm^{-1}, attributed to the out-of-plane bending vibration of C–H and the C–O-C vibration, respectively [16], show significant changes post-polymerization. The reduction in the intensity of the bending vibration peak (914 cm^{-1}), the redshift of the C–O-C vibration peak, and the emergence of a new chain vibration peak (845 cm^{-1}) [16,22] are indicative of the formation of a continuous PDOL polymer chain.

A battery comprises numerous interphases, including not only the well-concerned macroscopic interphases at the anode/electrolyte/cathode interfaces but also the critical microscopic interphases that exist between particles within the anode, solid electrolyte, and cathode, which are also essential for determining battery performance. *In-situ* polymerization can significantly enhance the contact at macroscopic interphases. Moreover, a gradual temperature increase during *in-situ* polymerization, slowly ris-

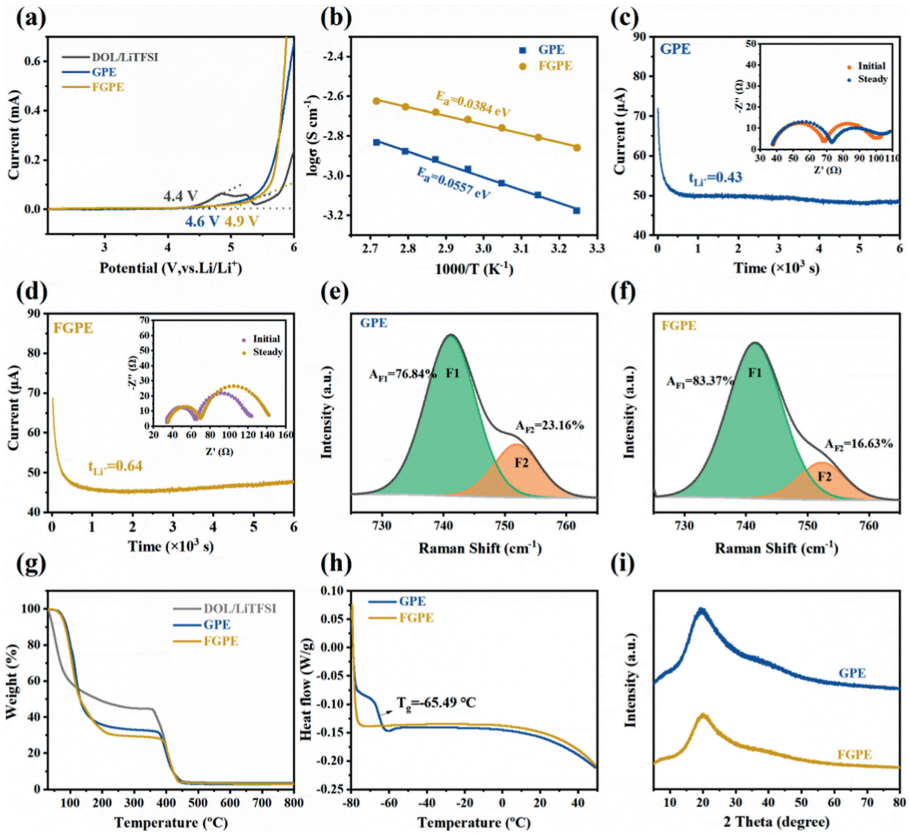


Fig. 2. An in-depth electrochemical and thermal analysis of the DOL electrolyte and its polymerized forms. (a) The electrochemical stability windows of the DOL/LiTFSI, GPE and FGPE. (b) The temperature-dependent ionic conductivity of GPE and FGPE, ranges from 30 °C to 90 °C. (c, d) The polarization curves along with the initial and steady-state impedance plots for Li|GPE|Li and Li|FGPE|Li cells. (e, f) Raman spectra, (g) TG analysis curve, (h) DSC analysis curves, and (i) XRD spectra of GPE and FGPE, offering insights into their structural and thermal properties.

ing from room temperature (12 h) to a mild 60 °C (4 h), facilitates the penetration of liquid monomers into the interstitial spaces between particles, thereby suppose to optimizing microscopic interphase contact. Additionally, this gradient temperature rise also promotes the homogeneity of GPE and FGPE by controlling the polymerization rate.

The utilization of ether electrolytes, particularly those represented by DOL, in high-voltage batteries is relatively uncommon owing to their susceptibility to oxidation at elevated potentials exceeding 4 V. In contrast, PDOL exhibits a markedly expanded electrochemical stability window. As evidenced by the linear sweep voltammetry (LSV) data depicted in Fig. 2a, the monomer exhibits an oxidation voltage of 4.4 V, while the GPE and FGPE can achieve a voltage of 4.6 V and 4.9 V (*vs.* Li/Li$^+$), respectively. The polymerization process effectively mitigates decomposition reactions, thus rendering it more viable for deployment under conditions of high voltage.

To further investigate the impact of FEC on Li$^+$ conduction, the ionic conductivity (σ) of both GPE and FGPE was measured across a temperature range of 30–90 °C (Fig. S2 and Table S1 in Supporting information). The ionic conductivity of GPE was found to be 0.67 mS/cm at 30 °C, which significantly increased to 1.38 mS/cm following the incorporation of FEC. This enhancement could be attributed to FEC's ability to facilitate the migration of PDOL polymer segments [23], thereby reducing the energy barrier for Li$^+$ transport. The relationship between ionic conductivity and temperature (σ-T) can be accurately described by the Arrhenius equation (Fig. 2b), allowing for the determination of the activation energy (E_a) of the electrolytes. The lower E_a of FGPE (0.0384 eV) is conducive to faster Li$^+$ conduction compared to GPE (0.0557 eV). Additionally, the presence of FEC improves the Li$^+$ transference number (t_{Li^+}) from 0.43 to 0.64 (Figs. 2c and d), likely due to enhanced chain mobility and increased availability of free Li$^+$ in FGPE.

Subsequently, Raman spectroscopy was employed to assess the degree of dissociation of the lithium salt LiTFSI (Figs. 2e and f). The Raman bands at 744 and 753 cm^{-1} correspond to the free TFSI$^-$ anion (F1) and Li$^+$-TFSI$^-$ contact-ion (F2), respectively [24,25]. In the GPE, the proportions of F1 and F2 are 76.84% and 23.16%, respectively. Notably, the ratio of F1 increases to 83.37% in FGPE, indicating a greater degree of dissociation of free Li$^+$ from LiTFSI following the introduction of FEC, which possesses a high dielectric constant [26]. For further investigation, we employed ^{7}Li nuclear magnetic resonance (NMR) spectroscopy using LiCl in D_2O as a capillary standard to assess the availability of Li$^+$ ions within the electrolytes (Fig. 1h). The chemical shift of free Li$^+$ is expected to be up-field shifted owing to the electron shielding effect of the coordinated solvent molecules. In comparison with DOL, the up-field shift observed for PDOL in the ^{7}Li NMR spectra suggests a higher availability of free Li$^+$ ions, particularly within the FGPE matrix. This indicates that PDOL may facilitate enhanced Li$^+$ mobility and contribute to improved electrolyte performance. However, it is essential to note that exceeding a certain threshold of FEC content can result in FGPE transitioning to a liquid state, thereby compromising interface stability and leading to a marked decrease in t_{Li^+} [23]. Consequently, the FEC content was maintained at 15% in this study.

Thermogravimetric analysis was conducted to evaluate the thermal stability of the investigated gel electrolytes (Fig. 2g). Specifically, weight loss was observed for both GPE and FGPE at a temperature exceeding 80 °C, whereas liquid DOL began to volatilize

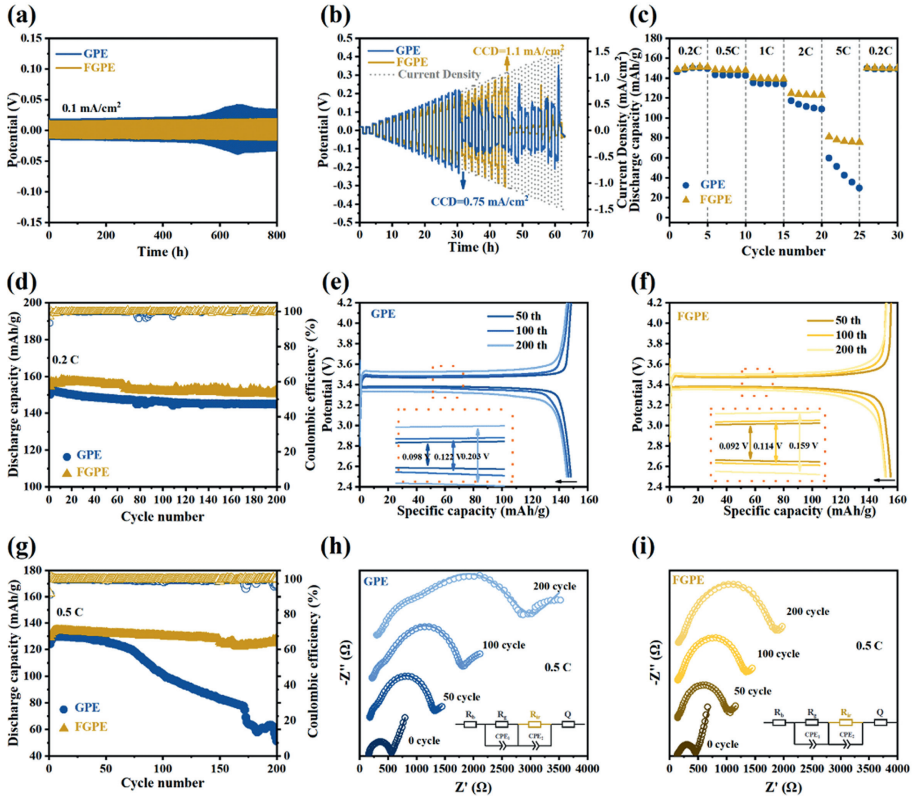


Fig. 3. A detailed examination of the electrochemical performance of batteries incorporating GPE and FGPE. (a) The constant current charge and discharge curves for Li-Li symmetrical cells with GPE and FGPE, operated at a current density of 0.1 mA/cm^2. (b) The charge and discharge curves of the two batteries at step current density. (c) The rate performance test, (d) the cycle performance test at 0.2 C, (e, f) the charge-discharge curves and polarization voltage changes (illustration) of different cycle numbers at 0.2 C, (g) the cycle performance test at 0.5 C and (h, i) the AC impedance patterns after 0, 50, 100, and 200 cycles, along with the equivalent circuit models (illustration) for full cells with GPE and FGPE, providing a comprehensive assessment of their electrochemical stability and performance over extended cycling. All the batteries were tested at 30 °C.

and decompose at approximately 30 °C. This observation suggests that the thermal stability of PDOL is enhanced following polymerization, with only a minimal amount of residual DOL remaining within the PDOL network. Fig. 2h presents the glass transition temperature (T_g) of PDOL, as measured by differential scanning calorimetry (DSC). The GPE exhibited a T_g of −65.49 °C, while the T_g of FGPE could not be detected due to the lower crystallinity of FGPE polymer. This finding aligns with the X-ray diffraction (XRD) data presented in Fig. 2i, which shows a lower peak for FGPE at approximately 20°, indicative of increased amorphous regions within the PDOL polymer chain segments. This suggests a significant enhancement in the mobility of FGPE, attributable to the addition of FEC, which possesses high ionic conductivity and facilitates rapid Li^+ conduction [27].

Given that the safety of the gel electrolyte is a critical concern for battery applications [28,29], the flammability of PVDF-HFP film and LLZO pellet impregnated with FGPE was examined (Fig. S3 in Supporting information). Due to the flame-retardant properties of FEC, neither of the two electrolytes with FGPE ignited. It is noteworthy that the inorganic solid-state electrolyte LLZO exhibits more excellent thermal stability and safety compared to the organic polymer electrolyte.

The reversibility of Li plating/stripping processes on Li metal electrodes was further investigated through electrochemical tests conducted on Li|Li symmetrical cells utilizing GPE and FEC-modified FGPE as interfacial layers. As illustrated in Fig. 3a, the cells, configured as Li|GPE|LLZO|GPE|Li and Li|FGPE|LLZO|FGPE|Li, were charged and discharged at a current density of 0.1 mA/cm^2 at room temperature. The overpotential observed in the cell with FGPE (∼14 mV) was marginally lower than that of the GPE cell (∼17 mV) prior to 550 h operation. Both cells exhibited stable lithium plating and stripping processes, maintaining low overpotential for 800 h This stability is attributed to the role of FEC in FGPE, which promotes the formation of a stable SEI film and facilitates uniform lithium deposition, thereby inhibiting the growth of lithium dendrites [30]. In contrast, the GPE cell experienced a significant increase in overpotential due to uneven lithium deposition. The critical current density (CCD) was measured to assess the practical application potential and dendrite-inhibition capabilities of FGPE (Fig. 3b). The CCD for GPE was determined to be 0.75 mA/cm^2, whereas the CCD for FGPE increased to 1.1 mA/cm^2.

Full cells utilizing GPE and FGPE as LLZO/electrode interlayers were assembled with commercial lithium iron phosphate $LiFePO_4$ serving as a cathode (Figs. 3c-g). Fig. 3c presents the discharge capacities of the cells structured as Li|FGPE|LLZO|FGPE|LFP and Li|GPE|LLZO|GPE|LFP, measured at various current rates. Both cells demonstrated the ability to recover their original capacity when cycled from 0.2 C to 5 C, and back to 0.2 C. The all-solid-state lithium metal battery employing FGPE exhibited superior rate performance, achieving discharge capacities of 148.13, 139.76, 124.63, and 80.84 mAh/g at 0.5, 1, 2, and 5 C, respectively, with minimal capacity attenuation. Conversely, the discharge capacity of the Li|GPE|LLZO|GPE|LFP cell declined rapidly at 5 C, reaching only 29.38 mAh/g after 5 cycles. These results underscore the significant enhancement in rate performance afforded by the inclusion of FEC as a solvent or additive, which is critical for the rapid charge and discharge capabilities of batteries. Fig. 3d illustrates the constant current charge-discharge cycle results of the full cells with GPE and FGPE at 0.2 C at RT. The initial specific discharge capacity of the Li|FGPE|LLZO|FGPE|LFP cell was 154.38 mAh/g, slightly

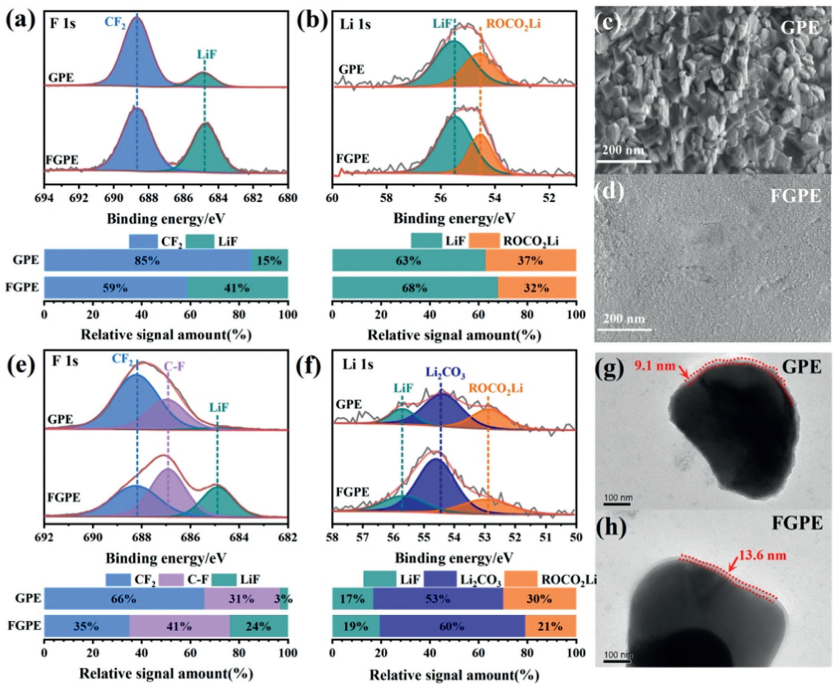


Fig. 4. An analytical overview of the anode and cathode surfaces of LFP/Li batteries post-cycling through XPS and electron microscopy techniques. (a) F 1s and (b) Li 1s XPS spectra derived from the anode surface after 20 cycles. (c, d) SEM images of the anode surface post-cycling. Similarly, (e) F 1s and (f) Li 1s XPS spectra, respectively, extracted from the cathode surface after 20 cycles. (g, h) TEM images of the cathode particles after 20 cycles.

surpassing that of the Li|GPE|LLZO|GPE|LFP cell, which recorded 150.08 mAh/g. The corresponding charge/discharge curves (Figs. 3e and f) indicate that the polarization voltage of the FGPE cell consistently remained lower than that of the GPE cell throughout the cycles. Furthermore, the excellent cycling performance of the Li|FGPE|LLZO|FGPE|LFP full cell at a higher current density of 0.5 C is demonstrated in Fig. 3g. The Li|FGPE|LLZO|FGPE|LFP cell exhibited an initial discharge capacity of 129.05 mAh/g with a capacity retention of 98.94%, whereas the Li|GPE|LLZO|GPE|LFP cell displayed only 41.36% capacity retention after 200 cycles. The findings illustrate that the cell utilizing FGPE demonstrates superior capacity and cycling stability compared to its GPE counterpart at elevated current densities.

To directly assess the improvement in interfacial contact and stability afforded by FGPE over GPE, EIS was performed on both cell configurations during cycling, with the Nyquist plots presented in Figs. 3h and i. The two semi-circles observed correspond to the grain boundary impedance (R_g) of LLZO and the interface impedance (R_{ir}) between LLZO and the electrode. Given that the LLZO component remains unchanged in both cells, the resistance difference primarily reflects variations in interface impedance. The smaller values of R_{ir} for the Li|FGPE|LLZO|FGPE|LFP cell, as compared in Fig. S4 (Supporting information), suggest that the use of FGPE, which possesses acceptable ionic conductivity and Li^+ transference number, significantly enhances all-solid-state lithium metal battery performance by promoting interfacial contact.

To further illustrate that the Li^+ conduction rate is enhanced by FGPE, the average lithium ion diffusion coefficient for both cells during charge and discharge was elevated using the constant current intermittent titration technique (GITT), as shown in Fig. S5 (Supporting information). The static voltage during all resting steps in the charge and discharge process was recorded at 3.43 V, indicating that the intercalation/deintercalation of Li^+ occurs at this potential. The Li|FGPE|LLZO|FGPE|LFP cell exhibited reduced ohmic polarization and a higher capacity retention rate during cycling, corroborating the previously mentioned cycling performance results. The higher lithium ion diffusion coefficients (D_{Li^+}) for the FGPE cell across various cycles are presented in Table S2 (Supporting information), indicating that the *in-situ* constructed FGPE accelerates Li^+ diffusion at the interface. For comparative analysis, Table S3 (Supporting information) summarizes the cycling performances of batteries utilizing polymer interlayers to modify the interface, highlighting the advantage of the LLZO/electrode interface modification strategy proposed in this study in terms of cycling performance at elevated current densities under typical operating temperatures.

A suite of analytical techniques, including XPS, SEM, and TEM, was employed to elucidate the impact of FEC on the formation and characteristics of SEI and CEI films in the FGPE cell. Post-cycling XPS analyses of the anodes revealed a pronounced LiF peak at 684.8 eV in the F 1s spectra for the FEC-containing electrolyte (Fig. 4a), indicative of a robust component, as corroborated by literature, which is considered a key component of the SEI film [20,31]. The diminished presence of the organic species $ROCO_2Li$ (Fig. 4b) implies enhanced stability throughout the charge-discharge cycles. The C–O and C=O peaks (Figs. S6a, c and d in Supporting information) correspond to the breakdown of the solvent. The migration dynamics of Li^+ at the interface may be accelerated in the FGPE-based battery, as the Li_2O species is found in the O 1s spectra for the cycled anode (Fig. S6b in Supporting information) [32]. SEM micrographs (Figs. 4c and d) of the cycled lithium metal anodes underscore the morphological differences; the FGPE-utilizing anode exhibits a smoother surface with minimal lithium dendrite formation, contrasting with the GPE anode, which is characterized by an uneven surface covered with dendrites. This observation suggests that an inferior SEI layer can precipitate non-uniform lithium deposition, thereby escalating the interfacial impedance and the likelihood of internal short circuits.

In the context of liquid lithium-ion batteries, FEC has been shown to contribute to the formation of a robust solid electrolyte interphase through processes of defluorination and decarboxylation. This contributes to the generation of LiF and Li_2CO_3 [33]. Sim-

ilarly, the influence of FEC extends to the formation of the CEI film at the cathode/electrolyte interface, as evidenced by the enhanced presence of LiF/Li_2CO_3 components in the presence of FEC (Figs. 4e and f). Although LiF is Li-insulating, the combined effect of LiF/Li_2CO_3 is posited to enhance the ionic conductivity and electronic insulation of the CEI, leading to the formation of a heterogeneous structure [34,35]. This synergistic effect is anticipated to augment the Li^+ diffusion coefficient and, consequently, the battery's rate capability. TEM analysis of the cycled cathodes (Figs. 4g and h) reveals a denser and more uniform CEI film on the surface of $LiFePO_4$ particles in the FGPE, which is conducive to efficient and homogeneous Li^+transport. This uniform coating is instrumental in safeguarding the cathode active material, curtailing electrolyte decomposition, and bolstering the battery's cycle life. Collectively, these findings underscore the beneficial role of FEC in FGPE, which simultaneously optimizes the SEI and CEI film compositions and structures, fostering a stable interphase for Li^+ conduction, ensuring uniform lithium plating, and mitigating side reactions during the cycling process.

In conclusion, a novel approach to modifying the interface between LLZO and electrodes through *in-situ* polymerization is presented. The FGPE incorporating FEC offers several notable advantages: Firstly, it facilitates the formation of a dense interface between LLZO and electrodes *via in-situ* polymerization, thereby establishing a uniform and rapid Li^+ transport pathway at the interface, which effectively reduces interfacial impedance. Secondly, the inherent non-flammability of FGPE significantly enhances the safety profile of lithium metal solid-state batteries by preventing thermal runaway events. Last but not least, the construction of an SEI film that is a composite of organic and inorganic components, along with a CEI enriched with LiF and Li_2CO_3, synergistically enhances the compatibility of the electrolyte with electrodes. This contributes to the uniform dissociation and deposition of Li^+, thereby suppressing the formation of lithium dendrites. The FGPE demonstrates an impressive ionic conductivity of 1.38 mS/cm and a Li-ion transference number of 0.64 at 30 °C. A Li|Li symmetric cell configuration utilizing the FGPE exhibits a high critical current density of 1.1 mA/cm^2, along with excellent cycling stability, maintaining a low polarization voltage for 800 h at 0.1 mA/cm^2. Additionally, the FGPE significantly enhances the rate capacity (80.54 mAh/g, 5 C) and cycling performance (98.94% capacity retention rate after 200 cycles at 0.5 C) of a Li|LFP full cell. In conclusion, while the FPGE has shown promising results, further optimization of the electrolyte's compatibility with commercial high-voltage layered cathodes is necessary to harness the energy density potential of all-solid-state batteries fully. Ongoing research is directed towards achieving this goal.

Declaration of competing interest

The authors declare that they have no known competing financial interests or personal relationships that could have appeared to influence the work reported in this paper.

CRediT authorship contribution statement

Xiaojin Wang: Writing – original draft, Formal analysis, Data curation. **Yi Chang:** Investigation, Funding acquisition. **Yuanyuan Zhang:** Writing – review & editing, Project administration, Funding acquisition. **Zhuohua Li:** Formal analysis, Data curation. **Haiqi Huang:** Software, Resources. **Yansha Huang:** Validation. **Jiawei Hu:** Validation. **Kai Zhang:** Writing – review & editing, Supervision. **Xuemei Gong:** Validation. **Ruirui Zhao:** Writing – review & editing, Supervision, Funding acquisition.

Acknowledgments

We acknowledge the financial support from the National Natural Science Foundation of China (No. 22105079), Natural Science Foundation of Guangdong Province (No. 2023B1515130004), Guangdong Basic and Applied Basic Research Natural Science Funding (Nos. 2023A1515010849 and 2024A1515012328), Key-Area Research and Development Program of Guangdong Province (No. 2024B1111080003).

Supplementary materials

Supplementary material associated with this article can be found, in the online version, at doi:10.1016/j.cclet.2024.110626.

References

[1] Z.F. Wang, J. Zhao, X.D. Zhang, et al., eScience 3 (2023) 100087.
[2] R.J. Chen, W.J. Qu, X. Guo, et al., Mater. Horiz. 3 (2016) 487–516.
[3] Y. Li, X.X. Liu, T. Ji, et al., Chin. Chem. Lett. 35 (2024) 109551.
[4] M. Zhang, X.X. Liu, J.D. Gu, et al., Chin. Chem. Lett. 34 (2023) 108471.
[5] K.V. Kravchyk, M.V. Kovalenko, Sci. Technol. Adv. Mater. 23 (2022) 2018919.
[6] F. Aguesse, W. Manalastas, L. Buannic, et al., ACS Appl. Mater. Interfaces 9 (2017) 3808–3816.
[7] S.N. Lauro, J.N. Burrow, C.B. Mullins, eScience 3 (2023) 100152.
[8] Z.H. Li, X.J. Wang, X.Y. Lin, et al., ACS Appl. Mater. Interfaces 15 (2023) 35684–35691.
[9] H.Y. Fan, F.X. Wei, J.C. Luo, et al., Sustain. Energy Fuels 5 (2021) 2077–2084.
[10] J.C. Chai, Z.H. Liu, J. Ma, et al., Adv. Sci. 4 (2017) 1600377.
[11] S.H. Zhang, F. Sun, X.F. Du, et al., Energy Environ. Sci. 16 (2023) 2591–2602.
[12] Q.Y. Wang, X.Q. Xu, B. Hong, et al., Energy Environ. Mater. 6 (2023) e12351.
[13] L. Wang, S.G. Xu, Z. Wang, et al., eScience 3 (2023) 100090.
[14] Y.X. Wang, T.Y. Li, X.F. Yang, et al., Adv. Energy Mater. 14 (2024) 2303189.
[15] H. Yang, M.X. Jing, L. Wang, et al., Nano-Micro Lett. 16 (2024) 127.
[16] Q. Zhao, X.T. Liu, S. Stalin, et al., Nat. Energy 4 (2019) 365–373.
[17] F.Q. Liu, W.P. Wang, Y.X. Yin, et al., Sci. Adv. 4 (2018) eaat5383.
[18] J.P. Zheng, W.D. Zhang, C.Y. Huang, et al., Mater. Today Energy 26 (2022) 100984.
[19] R. McMillan, H. Slegr, Z.X. Shu, et al., J. Power Sources 81 (1999) 20–26.
[20] X.Q. Zhang, X.B. Cheng, X. Chen, et al., Adv. Funct. Mater. 27 (2017) 1605989.
[21] D.Q. Liu, K. Qian, Y.B. He, et al., Electrochim. Acta 269 (2018) 378–387.
[22] J.Q. Zhou, T. Qian, J. Liu, et al., Nano Lett. 19 (2019) 3066–3073.
[23] W.H. Ren, Y.F. Zhang, R.X. Lv, et al., J. Power Sources 542 (2022) 231773.
[24] N. Chen, Y.J. Dai, Y. Xing, et al., Energy Environ. Sci. 10 (2017) 1660–1667.
[25] R. Rojaee, S. Cavallo, S. Mogurampelly, et al., Adv. Funct. Mater. 30 (2020) 1910749.
[26] K.R. Deng, Q.G. Zeng, D. Wang, et al., Energy Storage Mater. 32 (2020) 425–447.
[27] X.Y. Zhang, C.K. Fu, S.C. Cheng, et al., Energy Storage Mater. 56 (2023) 121–131.
[28] Y. Cui, J.Y. Wan, Y.S. Ye, et al., Nano Lett. 20 (2020) 1686–1692.
[29] Q.S. Wang, L.H. Jiang, Y. Yu, et al., Nano Energy 55 (2019) 93–114.
[30] Y.L. Liu, Y.L. Xu, Chem. Eng. J. 433 (2022) 134471.
[31] J. Tan, J. Matz, P. Dong, et al., Adv. Energy Mater. 11 (2021) 2100046.
[32] H.P. Zeng, K. Yu, J.W. Li, et al., ACS Nano 18 (2024) 1969–1981.
[33] I.A. Shkrob, J.F. Wishart, D.P. Abraham, J. Phys. Chem. C 119 (2015) 14954–14964.
[34] Q.L. Zhang, J. Pan, P. Lu, et al., Nano Lett. 16 (2016) 2011–2016.
[35] Z. Liu, Y. Qi, Y.X. Lin, et al., J. Electrochem. Soc. 163 (2016) A592–A598.